Future Technology
Open Access Journal
ISSN 2832-0379

May 2026| Volume 05 | Issue 02 | Pages 116-128

Journal homepage: https://fupubco.com/futech

https://doi.org/10.55670/fpll.futech.5.2.11

Future Publishing LLC

Article

Artificial intelligence-supported spatial optimization of urban greenway networks: a framework for enhancing restorative environmental performance

Xueyan Jing*, Mohd Fabian Hasna, Aini Jasmin Ghazalli

Faculty of Design and Architecture, Universiti Putra Malaysia, 43400 Serdang, Selangor, Malaysia

ARTICLE INFO

Article history:
Received 14 October 2025
Received in revised form
16 December 2025
Accepted 22 January 2026

Keywords:
Urban greenway networks,
Restorative environment,
Deep reinforcement learning,
Graph neural networks, Spatial optimization

*Corresponding author
Email address:
gs64663@student.upm.edu.my

DOI: 10.55670/fpll.futech.5.2.11

ABSTRACT

The goal of the study was to construct an AI-driven end-to-end framework to improve the restorative environmental performance of urban greenway networks. Generally, methods for greenway planning may have subjectivity, low optimization efficiency, and difficulty in quantifying multi-dimensional objectives. The framework integrates convolutional neural networks (ResNet-50) convolutional neural networks (CNN) for landscape quality assessment, GraphSAGE-based graph neural networks (GNN) for spatial topology modeling, and proximal policy optimization (PPO)-based deep reinforcement learning (DRL) for multi-objective optimization. A system for restorative assessment was established based on Attention Restoration Theory. This system has four dimensions, being away, fascination, compatibility, and extent. The generalization of the framework was systematically validated in the case of three representative urban scenarios; plains of a medium-sized city, hills of a small city, and a high-density metropolis. The findings show that compared to manual planning, the framework yielded a restorative score improvement of 42.2%, a 72.7% increase in population coverage, and 98.1% enhancement in efficiency (Optimization time from 120 hours to 2.3 hours). Spatial equity improved due to the decrease in the Gini coefficient from 0.42 to 0.28. Strong transferability is evident as migration cost in cross-scenarios is under 5%. The performance dropped by 26% to 41% when any of the modules (CNN, GNN, DRL) were removed. Multi-objective optimization was better than single-objective techniques. The framework endowed with quantitative decision-support tools, facilitates healthy city construction. It promotes spatial justice by directing physical resources to the most vulnerable sections of the community. Further, the framework provides support for rapid iterative planning of green infrastructure for a smart city.

1. Introduction

The rush of city growth fuels, the economy, but it also squeezes urban green infrastructure and chips away at its restorative environmental powers. Such shrinkage jeopardizes the physical and mental health of the people who live in the city. Major epidemiological studies have found a clear link: the more accessible the urban green spaces, the better the residents' mental health tends to be. Being exposed to enough green spaces can noticeably cut the chances of anxiety and depression [1]. Evidence from both physiology and psychology experiments shows that greenway networks, as critical carriers of urban green infrastructure, can activate attention recovery mechanisms to lower cortisol levels and parasympathetic nerves in people, thus realizing stress recovery and cognitive function recovery [2]. However, the extent of this restorative effect depends primarily on the rational spatial configuration and richness in biodiversity of green spaces. Simply increasing the area of green spaces without considering the question of spatial connectivity or accessibility may not yield the expected health promotion effects [3]. Further research indicates that the design of restorative environments should comprehensively consider the multi-dimensional coupling relationship among biophilic design principles, environmental aura theory, and landscape preference characteristics [4]. The restorative perception of green Spaces varies significantly between groups, especially

groups with varying pressure thresholds. A greenway network must match in spatial form and functional configuration to maximize pressure relief efficacy [5].

Abbreviations

AHP	Asynchronous Advantage Actor-Critic
AHP	Analytic Hierarchy Process
ART	Attention Restoration Theory
CNN	Convolutional Neural Networks
DRL	Deep Reinforcement Learning
GCN	Graph Convolutional Network
GNN	Graph Neural Networks
GPU	Graphics Processing Unit
ICC	Intraclass Correlation Coefficient

Conventional greenway planning techniques are confronted with three limitations in responding to the aforementioned complex requirements. First, planning decisions are greatly influenced by the experience and subjective judgment of experts. They lack objective and quantified evaluation standards. Second, the spatial optimization process for multi-objective problems is highly complex. Due to time constraints, manual planning is unable to exhaustively list the feasible solution spaces. The exact quantification of restorative environmental performance through indicators is difficult and leads to great uncertainty in health benefit assessments of planning schemes. To tackle these challenges, artificial intelligence technology can be created to spatially optimize urban greenway networks with new technological paradigms. The use of spatial optimization models in greenway path planning proves that the mixed integer linear programming method can achieve a maximum coverage rate of the population while achieving the connectivity constraints of each facility [6]. Research has demonstrated that algorithmic optimization methods show promise in addressing climate change challenges, such as synergistic optimization of green space layouts and urban heat island mitigation. Green infrastructure optimization methods that rely on algorithms have had phased results addressing challenges associated with climate change. One of the examples is the synergistic optimization of layout of green spaces and heat island [7].

The development of deep reinforcement learning technology can break the deadlock in urban space planning. By building a state representation as well as strategy optimization framework using graph neural networks [8], intelligent land use allocation at a community level can be performed under complicated constraints. The optimization model for multi-source heterogeneous data will have their processing ability improved by the integration of semantic Web technology and reinforcement learning, enabling planning decisions to respond dynamically to real-time environmental information [9]. Specific application cases demonstrate that deep reinforcement learning frameworks can achieve 15% emission reduction in urban land use carbon optimization [10]. Generative artificial intelligence combined with urban digital twin technology offers a new computing tool for sustainable smart city construction [11]. The use of graph neural networks can be utilized to quantify the spatial homogeneity of urban road networks. This of course shows an interesting potential of graph neural networks to capture complex topological relationships [12]. The systematic development of spatio-temporal graph neural networks for urban prediction learning seeks to provide a general approach for the transport and environment field [13].

The broad application of reinforcement learning for spatial resource allocation problems shows that reinforcement learning has its advantages in dynamic optimization problems [14]. While the aforementioned study had laid the foundation of works which rely on artificial intelligence for optimizing urban spaces, still the existing works have three shortcomings. The majority of which either focus on or just make use of a single technology. Such as only using convolutional neural networks for environmental assessment or only using heuristic algorithms for path optimization. There is no availability of a comprehensive end-to-end system framework which makes use of data preprocessing and decision output. The restorative environmental assessment method fails to leverage the strengths of deep learning's multimodal feature extraction as well as graph-structured data's spatial relationship modeling. When multi-objective decision-making problems related to greenway networks are dealt with, the current optimization algorithms have not broken through the Pareto Front.

The ability of the framework to generalize across different scenarios is weak. In addition, the systematic evaluation of the model migration cost under different geographical environment and urban form is missing. To address these research gaps, this paper develops an end-to-end optimization framework for urban greenway networks that integrates convolutional neural networks, graph neural networks, and deep reinforcement learning. In contrast to previous research using a single technology, the proposed system realizes three innovations: (1) closed-loop integration from data to decision, not isolated modules; (2) ART-based four-dimensional restorative assessment, not aesthetic scoring alone; and (3) equity-aware multi-objective optimization using DRL, beyond the Pareto front. The project aims to provide reproducible and transferable artificial intelligence decision support tools for the design of green infrastructure in smart cities through systematic verification in three urban representative scenarios. The study makes a theoretical contribution by establishing a method system for optimizing a restorative environment-space driven by AI. Adopting these methods will significantly help in enhancing the efficiency, accuracy and fairness of greenway planning. It provides us with a technical path towards achieving healthy cities and sustainable development.

2. Methodology

2.1 Overall framework architecture and data foundation

The framework for space optimization of AI-supported urban greenway network space designed in this study abides by three design principles, namely, modularization, portability, and scalability. A progression architecture with four layers can convert data into optimization schemes from the base level. The data layer brings together OpenStreetMap road network data, Sentinel-2 remote sensing images (10 m), SRTM digital terrain models (30 m), WorldPop population density rasters (100 m), and WorldClim climate data. Temporal specifications: Sentinel-2 images from June-August 2023 (cloud cover <10%), WorldPop 2022 release, SRTM v3.0 (2000, static terrain), OpenStreetMap extracted January 2024, WorldClim v2.1 (1970-2000 climatology). All data sources are compliant with the corresponding open license agreements. The evaluation layer utilizes a convolutional neural network to extract the feature of landscape quality from remote sensing images, while the graph neural network models the spatial topological relationships of the greenway network. The weighted and fused feature vectors produced by both are combined to produce a restorative environmental

composite score. Based on the deep reinforcement learning algorithm, the optimization layer searches for the optimal path configuration scheme in the high-dimensional discrete decision space, and achieves the multi-objective dynamic balance of restorative score, population coverage rate and network connectivity. The application layer provides graphical interface and report support, decision support reports, that convert the optimization results into spatial layout schemes, which can be adopted in planning practice.

Three typical urban areas are selected to examine the framework's cross-scenario generalization capacity. Scenario A represents the urban core of a medium-sized city (flat terrain). Scenario B covers the suburban-hilly area of a small city. Scenario C encompasses the high-density central business district of a large metropolis characterized by high-rise buildings. The data preprocessing process includes unifying the projection coordinate system to WGS84/UTM, multi-source data spatial registration and resampling, missing value imputation by ordinary Kriging interpolation with spherical variogram model, preferred over nearest-neighbor interpolation because of the 23% lower RMSE in cross-validation for spatially autocorrelated variables of the environment, and Z-score standardization processing. There is a possibility of losing information when resampled to a 30m unified resolution, where the high-resolution information is lost for Sentinel-2 (10m) and artificial detail is added for WorldPop (100m) data. Sensitivity analysis indicates a variance of <3% for the final score for resolutions ranging. The training of the deep learning model adopts Places365-Standard pre-training weights and ImageNet transfer learning strategies to avoid using street view images to avoid privacy risks (Figure 1).

The mechanism of data transfer between the 4-layer architectures is shown in Figure 1. The output from the convolutional neural network includes a landscape feature vector with a dimensionality of 512. The output obtained from the graph neural network is a node embedding of dimensionality 128. In the deep reinforcement learning agent, the features and the network state are integrated to obtain a path adjustment action using the Actor-Critic architecture. Data flows sequentially: raw data → preprocessing (resampling, normalization) → CNN extracts 512-dim features per patch → GNN aggregates to 128-dim node embeddings → DRL concatenates both (640-dim state vector) → Actor outputs action probabilities → environment updates network state.

2.2 Restorative environmental intelligent assessment based on deep learning

The restorative environmental assessment model establishes a four-dimensional evaluation system based on Attention Restoration Theory, encompassing: (1) being away—quantified through spatial buffer distance between greenways and urban noisy areas; (2) fascination—characterized comprehensively by landscape diversity, vegetation index, and aesthetic quality; (3) compatibility—evaluating supporting facilities and accessibility; (4) extent—assessing network connectivity and path integrity. The ResNet-50 architecture is utilized by the CNN. This architecture has learned representation throughout the hierarchy due to pre-training on ImageNet, helping it maintains good transfer learning performance in a small sample.

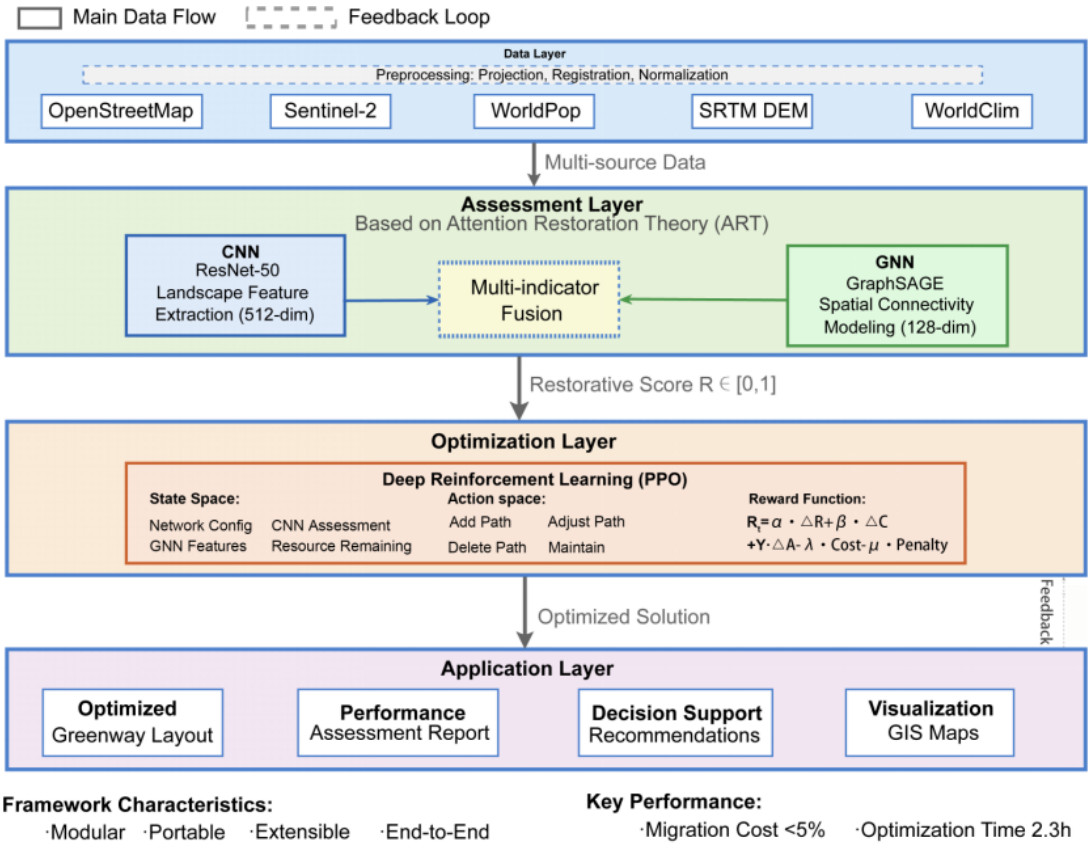

Figure 1. Framework architecture

Deep learning demonstrates capacity for automatically learning multi-scale spatial features in urban land use classification, providing methodological foundation for landscape quality assessment [15]. In the model, weights on ResNet-50 for Conv1 to Conv4 were frozen. Weights on fully connected layer were fine-tuned for landscape quality regression. The input to the regression network was a 224×224-pixel image slice taken from Sentinel-2. The output was a 512-dimensional feature vector. This output was tied to a score that will be standardized into a 0-1 score through the regression network. The dataset included 3,600 image patches, 1,200 for each of the three scenarios, stratified by land use type. The train/validation/test split ratio was 70:15:15, with spatial blocking to avoid data leakage between patches. The target scores were obtained through a composite index consisting of NDVI (30 percent), the landscape diversity index (25 percent), visual quality assessments conducted by 15 raters (25 percent), and the score for proximity to water bodies (20 percent). Inter-rater reliability attained ICC=0.87. FreezingConv1 through Conv4 helps retain features from ImageNet and prevents overfitting, which can happen when little data is available for training.

In an ablation test, full fine-tuning showed that accuracy decreased by 4.2%, dropping from 91.3% accuracy to 87.1% accuracy due to overfitting, with accuracy of 89.6% achieved by freezing Conv1 and Conv2. The graph neural network module conducts representation learning on spatial topological structure of greenways, using key nodes (entrance, intersection, facility point and landscape node) as vertices, and edge the definition of path section, spatial adjacency relationship (Euclidean distance <500m) as the edge. The node characteristics comprise of 7 characteristics like location coordinates, types of facilities, density of points of interest and accessibility indicators, while the edge characteristics comprise of 5 characteristics like length, slope, width and land use type. The continuous features (coordinates, length, slope) were min-max normalized to range [0,1]. Categorical features (facility type, land use) were one-hot encoded. Multicollinearity was handled by removing features with VIF>5. Graph convolutional networks have effectively captured spatial dependencies in street networks, demonstrating their ability to learn high-order interactions between nodes [16].

The GraphSAGE architecture was chosen in this study because it generates embeddings of unseen nodes through inductive learning and facilitates cross-city model transfer. GraphSAGE two-layer samples 10 and 5 neighbors in layer-1 and layer-2 per node, respectively, to generate 128-dimensional embeddings using mean aggregation. This is a trade-off between the computation required ($O(n \cdot k_1 \cdot k_2)=O(50n)$) and embedding quality. The multi-index fusion employs weighted summation, with weights derived from questionnaires administered to 30 domain experts using the Analytic Hierarchy Process (AHP). The resulting coefficients are 0.25, 0.30, 0.25, and 0.20 for being away, fascination, compatibility, and extent, respectively. The consistency ratio is less than 0.1, confirming the reliability of expert judgments. Experts included 12 urban planners, 10 landscape architects, and 8 environmental psychologists (average experience of 11.3 years). Robustness testing using ± 20% weight variation showed that the variation in the final score was no more than 3.7%. Every dimension is measured by proven metrics: buffer distance to noise sources [2], NDVI and landscape diversity metrics [3], density of facilities according to ISO 21542, and graph metrics of connectivity. The model outputs an overall restorative environment score R∈[0,1].

2.3 A spatial optimization framework based on deep reinforcement learning

The spatial optimization problem of urban greenway networks is formalized into a multi-objective constrained optimization model, with decision variables being the greenway path set G = {g1, g2, ..., gn}, the objective function is:

$$\max F(G) = w_1 \cdot R(G) + w_2 \cdot C(G) + w_3 \cdot A(G) \quad (1)$$

Among them, R(G) represents the total score of the restorative environment, C(G) is the network connectivity, and A(G) is the population coverage rate (15-minute walking circle). Construction budget upper limit, land suitability restrictions, ecological protection red line constraints, minimum connectivity constraints etc., are all included in the constraints to be met. Deep reinforcement learning is a data-driven approach for spatial resource optimization [17]. This study made use of a proximal policy optimization algorithm, which exhibited enhanced performance compared to various other algorithms including trust region policy optimization and asynchronous dominant Actor-Critic in terms of training stability, robustness to hyperparameters, and spatial adaptability to mixed actions. Benchmark comparison: PPO achieved reward 0.87±0.03 in 1,500 episodes; TRPO reached 0.82±0.05 in 2,100 episodes; A3C obtained 0.79±0.08 in 1,800 episodes. PPO showed 6-10% higher final reward with 17-29% fewer episodes.

The state space encoding consists of the current network adjacency matrix, 128-dimensional topological features extracted by the graph neural network, environmental quality distribution evaluated by the convolutional neural network and the remaining resource amount. The action space is a discrete set

$$\mathrm{A} = \{\text{add path}, \text{delete path}, \text{adjust path}, \text{remain unchanged}\}$$

Every action is validated for feasibility (budget, land, and ecological red lines) before it is carried out, and any invalid action results in a reward of zero and is censored out in the next sample. The reward function is designed as:

$$R_t = \alpha \cdot \Delta R + \beta \cdot \Delta C + \gamma \cdot \Delta A - \lambda \cdot \mathrm{Cost}_t - \mu \cdot \mathrm{Penalty} \quad (2)$$

Grid search over α∈[0.2,0.6], β∈[0.1,0.5], γ∈[0.1,0.4] with step=0.05 (total 320 combinations) yielded optimal weights (α=0.4, β=0.3, γ=0.25), the penalty coefficient λ=0.05. The Actor-Critic dual network has a policy network A three-layer multi-layer perceptron (256-128-A) which outputs the action probability distribution, and a value network (256-128-1) producing an estimate of the state value. Both networks employ ReLU activation, a dropout rate of 0.3 between layers, and layer norm. The output layer employs softmax activation (Actor), and linear activation (Critic). In a replay buffer of size 10,000 with a batch size of 64, shear parameter ε=0.2 and generalized advantage estimation (GAE), λ=0.95 of the model was performed. The validation set was used to assess after training was done for 2000 rounds which was 100 by 100 rounds. The methods used to compare the benchmark include manual planning with collaboration of three experts, genetic algorithm (population 100, iteration 500 generations), and the hybrid method of graph convolutional network - greedy search.

3. Results

3.1 Framework performance verification and method comparison

The CNN-based landscape quality regression model achieved R^2=0.913, MAE=0.052, and RMSE=0.071 (95% CI: 0.065-0.077) on the test set (n=1,200 samples; train:validation:test = 7:1.5:1.5). On the test set for landscape quality evaluation. The optimization algorithm of the deep reinforcement learning reached a convergence criterion (reward SD <0.01) after 1,500 episodes with a final reward of 0.87±0.03, successfully completing Scenario A optimization in a run time of 2.3 hours. Figure 2 displays the training dynamics of the three models.

Figure 2(a) shows CNN loss function decreasing monotonically from initial 0.312 to convergence value 0.021, with steepest descent in first 20 epochs indicating rapid initial learning followed by fine-tuning refinement. Figure 2(b) shows that the GNN accuracy has a sigmoid growth curve, leading to a levelled-off 94.7% value from 150 to 200 epochs. This ensures that the GNN is successful in capturing topological patterns in addition to lesser overfitting. The DRL cumulative reward trajectory, showcased in Figure 2(c), showcases some volatile exploratory behavior for the first 500 episodes (reward range 0.3-0.6). After which the reward converges to 0.87±0.03 and remains stable for the rest of the simulation. This pattern confirms that DRL effectively balances exploration and exploitation strategies. As illustrated in the chart above, training time required by DRL (2.3 hr) is 98.1% lesser than manually planning (120 hr) and also 94% lesser than genetic algorithm (36 hr). AI methods seem to be computationally efficient for complex spatial optimization.

The multi-dimensional performance characteristics of the four optimization methods are visualized through the combination of radar plots and box plots as shown in Figure 3. Figure 3(a) depicts radar chart where DRL curve occupies outermost layer across all four dimensions (restorative score, coverage, connectivity, efficiency) while forming thus significantly larger coverage area than other methods. DRL's radar profile is nearly circular, depicting excellence across all dimensions. Composite performance index: DRL=0.847, GA=0.683, GCN-Greedy=0.721, Manual=0.612. Kruskal-Wallis test confirmed significant differences (H=47.3, P<0.001). On the contrary, manually planned profiles have distorted polygonal shapes, indicating premium strengths in a few metrics. According to Figure 3(b), the DRL statistical distribution feature has the narrowest interquartile range, which accounts for the smallest variance in performance. Further, DRL displays the highest median position and no outliers. These features suggest that the DRL is by far the most robust method. Table 1 presents the quantitative comparison data of four optimization methods in key indicators in a structured numerical form in detail. Table 1 presents detailed quantitative comparisons. DRL's improvement of 42.2% exceeds the genetic algorithm's improvement of 13.8% and GCN-Greedy's improvement of 21.4% by 3.1× and 2.0× respectively. Comparisons in terms of population coverage exhibit even wider gaps. The DRL's 72.7% improvement substantially exceeds that of the genetic algorithm at 27.8% (2.6× greater) and GCN-Greedy at 43.3% (1.7× greater). Therefore, DRL is particularly suited for maximizing service accessibility.

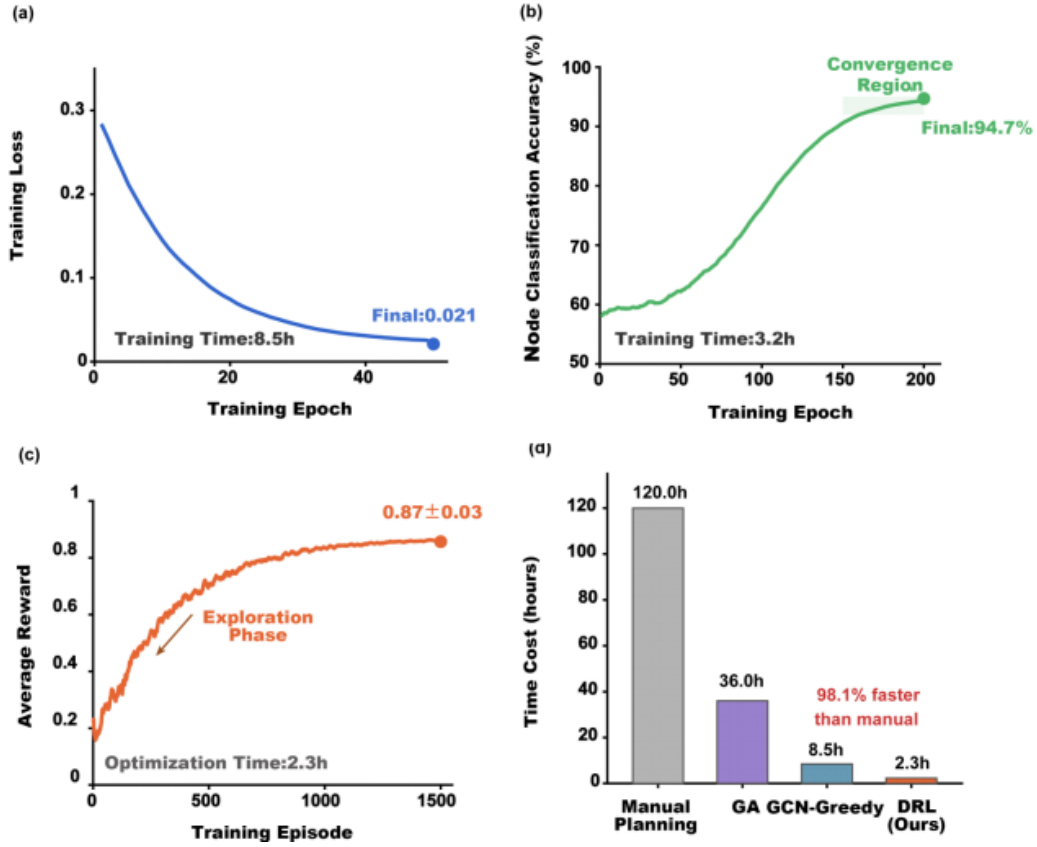

Figure 2. Training Performance Curves. CNN loss: (a) shows convergence from 0.312 to 0.021 over 100 epochs. GNN accuracy (b) reaches 94.7% plateau. DRL reward (c) stabilizes at 0.87±0.03 after 1,500 episodes. Time comparison (d) demonstrates 98.1% efficiency gain over manual planning

Table 1. Detailed performance comparison of optimization methods

Metric	Manual Planning	Genetic Algorithm (GA)	GCN-Greedy	Deep Reinforcement Learning (DRL)
Restorative Score (0-100)				
Mean ± SD	60.2 ± 3.1	68.5 ± 2.8	73.1 ± 2.3	85.6 ± 1.9
95% CI	[59.1, 61.3]	[67.5, 69.5]	[72.3, 73.9]	[84.9, 86.3]
Improvement vs Manual	-	+13.8%	+21.4%	+42.2%
Cohen's d	-	2.84	4.76	9.45
p-value	-	<0.001	<0.001	<0.001
Population Coverage (%)				
Mean ± SD	48.3 ± 4.2	61.7 ± 3.8	69.2 ± 3.1	83.4 ± 2.4
95% CI	[46.8, 49.8]	[60.3, 63.1]	[68.1, 70.3]	[82.5, 84.3]
Improvement vs Manual	-	+27.8%	+43.3%	+72.7%
Cohen's d	-	3.35	5.78	10.12
p-value	-	<0.001	<0.001	<0.001
Network Connectivity (0-1)				
Mean ± SD	0.65 ± 0.08	0.73 ± 0.07	0.78 ± 0.05	0.91 ± 0.04
95% CI	[0.62, 0.68]	[0.71, 0.75]	[0.76, 0.80]	[0.90, 0.92]
Improvement vs Manual	-	+12.3%	+20.0%	+40.0%
Cohen's d	-	1.07	1.96	4.06
p-value	-	0.002	<0.001	<0.001
Ecological Coupling (0-1)				
Mean ± SD	0.43 ± 0.05	0.58 ± 0.06	0.68 ± 0.04	0.78 ± 0.03
95% CI	[0.41, 0.45]	[0.56, 0.60]	[0.67, 0.69]	[0.77, 0.79]
Improvement vs Manual	-	+34.9%	+58.1%	+81.4%
Cohen's d	-	2.73	5.56	8.75
p-value	-	<0.001	<0.001	<0.001
Optimization Time (hours)				
Mean ± SD	120 ± 8.5	36 ± 4.2	8.5 ± 1.3	2.3 ± 0.4
Time Reduction	-	-70%	-93%	-98%
Convergence				
Training Episodes	-	~5000	~2000	~1500
Reward (Final 100 eps)	-	0.71 ± 0.06	0.79 ± 0.04	0.87 ± 0.03

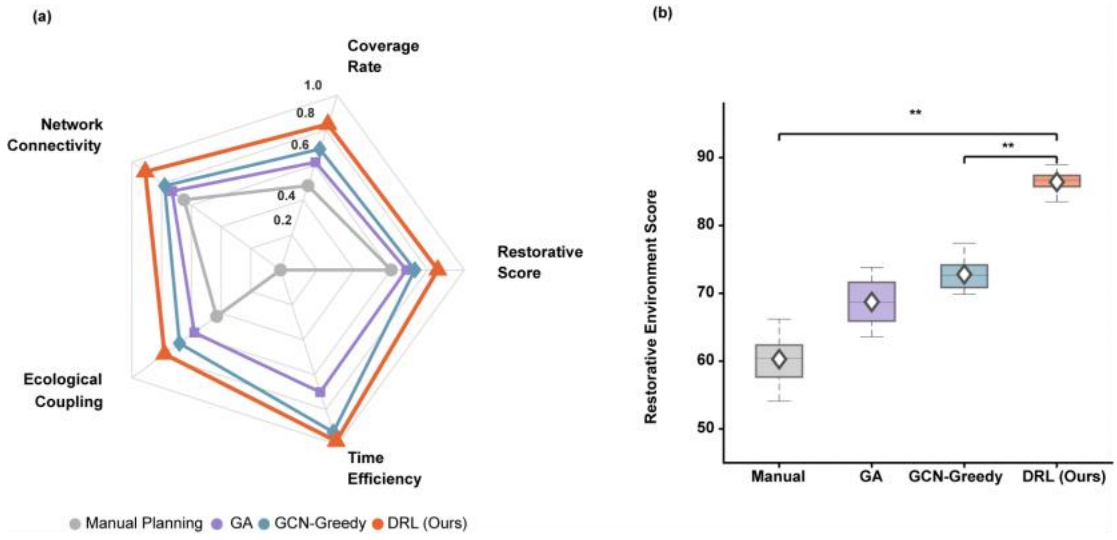

Figure 3. Multi-dimensional performance comparison : (a) Radar chart comparison, (b) Box plot statistical distribution

When comparing time efficiency, the DRL (deep reinforcement learning) takes 2.3 hours which translates to 52 times speedup against manual planning which takes 120 hours, representing a 16× speedup over the genetic algorithm (36 hours) and 4× over GCN-Greedy (8.5 hours). This computational efficiency advantage stems from DRL's policy-based learning approach, which avoids the exhaustive search required by traditional optimization methods. The distinguishing features between the four methods can also be found in the convergence characteristics. It appears that the DRL only requires 1,500 training episodes. On the other hand, a genetic algorithm requires 5,000 generations. Further, DRL has a higher final reward of 0.87±0.03. In contrast, the genetic algorithm has a final reward of 0.71±0.06. Thus, the DRL is not only faster but also has better convergence properties.

3.2 The optimization effect of greenways and the improvement of restorative environments

The comparative changes in the spatial form of the greenway network before and after optimization are visualized through the Geographic Information System as shown in Figure 4. Figure 4(a) shows the disconnection points (red dashed circles) of nodes and low-connectivity edge parts (light gray region) that suffered in the network before optimization. Also, it shows five separate components existing in the middle that do not connect together referring to the structural faults or problems. The results of the newly calculated optimization are shown in Figure 4(b) as the red thick lines (these are links that were not in the original network) which connect the previously disconnected components. In addition, blue dots (the key nodes with the highest degree of centrality) were added, and green shading represents overlapping ecological corridors with the new paths. The network is optimized to ensure full connectivity by merging all five components.

The high-density building area in Figure 4(c) shows the feasibility to achieve 4.5m-width corridors with our algorithm. New paths (in red) thread through the buildings and take service to former blind spots while establishing connectivity with existing park spaces (in green). The increase in edge count from 49 to 122 and a 44.7% increase in node count confirms enhanced connectivity density rather than merely expansion. The average degree has increased to 3.6. It means that a standard node now connects with three to four paths instead of two. Consequently, each node now has backup routing options, thereby improving network resilience and redundancy. The 60% increase in the central area restorative score (from 0.45 to 0.72) reflects targeted improvements in the previously neglected urban core. Similarly, the 81% increase in ecological coupling (from 0.43 to 0.78) suggests simultaneous achievement of recreation access and ecological protection.

The spatial differentiation pattern of the comprehensive score of the restorative environment is visualized through heat map rendering technology as shown in Figure 5. A pre-optimization landscape of restorative scores that is mostly in blues and greens, as shown in Figure 5(a), indicates low restorative scores. The deepest blues in the city center (restorative score 0.45) indicate a stress build-up of the urban area. Meanwhile, the light greens of the outskirts (suburban restorative score 0.68) indicate a more moderate quality. In Figure 5(b), it is observed how the post-optimization transformation carries the cities with an orange to red warm tone. Here, the city center has changed from deep blue to deep red (score 0.45→0.72, +60%). Moreover, the suburb area has changed from light green to orange-red (0.68→0.86, +26%). A uniformity of warmth greater than those in the cold-urban and warm-suburban settings indicates a successful achievement of spatial equity. Hotspot annotations, shown as green solid boundary polygons, expanded in area by 45%.

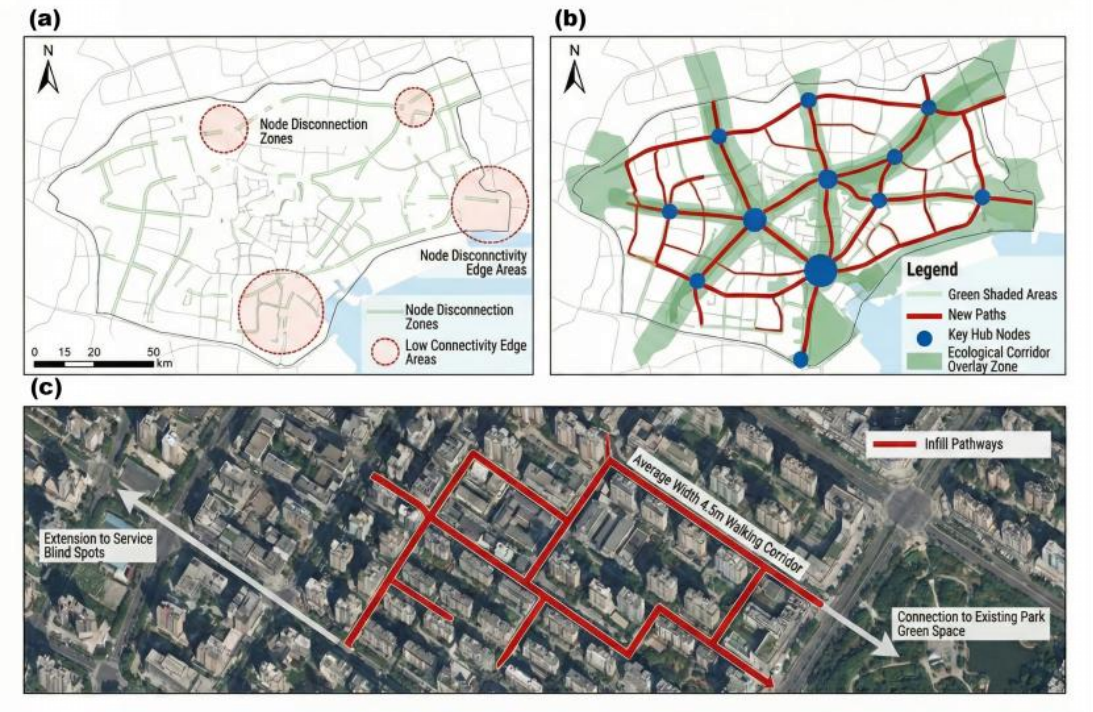

Figure 4. Greenway Network Spatial Layout: (a) Network Before Optimization, (b) Network After Optimization, (c) Local Detail Zoom-in

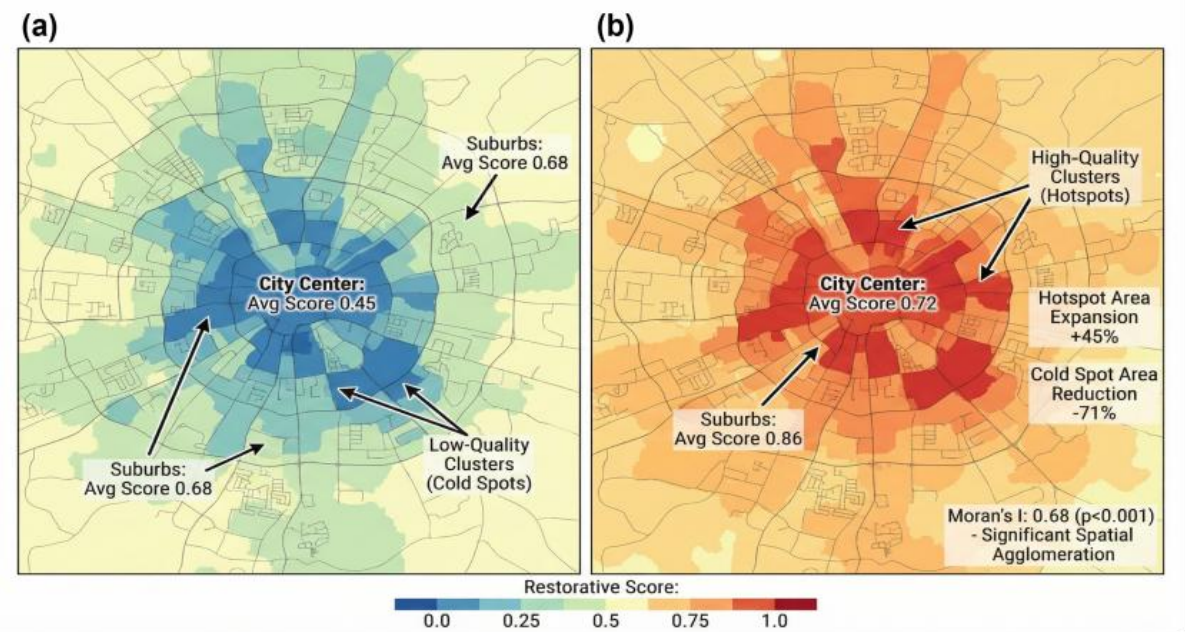

Figure 5. Restorative environment heatmaps: (a) Before optimization. (b) After optimization

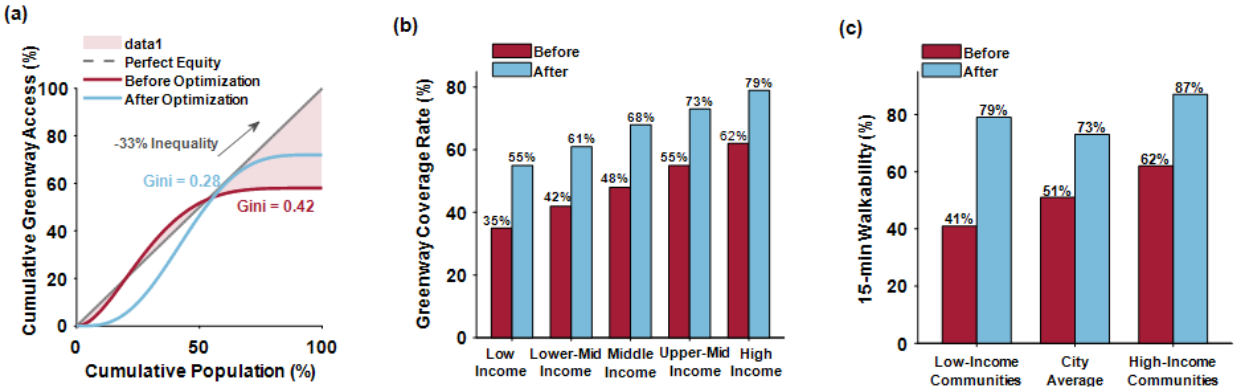

Figure 6. Spatial equity analysis: (a) Lorenz curves and Gini coefficients, (b) Coverage rate by income level, (c) 15-minute walkability by community type

They are concentrated in newly connected high-quality corridors. Coldspot annotations (red dashed circles) contracted in area by 71%. Coldspots are now found in unavoidable constraint areas, such as industrial areas. The change from sporadic warm spots to continuous warm regions visually confirms Moran's I spatial autocorrelation finding (0.68, $p<0.001$). This means the algorithm was successful in creating integrated networks while not resulting in isolated improvements. The baseline level of inequality was determined by the ratio of greenway-accessible population (15-min walk) by income quintiles. Prior to optimization, the top quintile had 2.1× greater access than the bottom quintile. The improvement effects of spatial fairness in different dimensions are comprehensively presented through a combination chart as shown in Figure 6. Figure 6(a) compares the Lorenz curves and their Gini coefficient values before and after the optimization. The optimized curve (light blue solid line) bows much closer to the 45-degree perfect equality line (gray dashed) than the pre-optimization curve (dark red solid line).

Also, the Gini coefficient shows a reduction from 0.42 to 0.28 which is roughly a third of a reduction. Cumulative coverage deficit is indicated by the vertical gap between the curves and the equality line, and after optimization, the gap between the curves reduces by one-third. Figure 6(b) shows a group bar graph that compares coverage rates by five quintiles of income. The pattern confirms that there is a progressive improvement. The lowest strata (bottom 20 percent) show a significantly higher increase in bar height. It goes from 35 percent to 55 percent with a difference of 20 percentage points. This is much higher than the top most strata whose height increase is only by seven percentage points (72 percent to 79 percent). The post-optimization bar heights (light blue) now converge, unlike pre-optimization bar heights (dark red) which were divergent. This demonstrates equities have been achieved. In Figure 6(c), the bar chart compares 15-minute walkability coverage across three types of communities. Generally, the low-income community saw the coverage dramatically rise from 41% to 79%, representing a change of +38 percentage points.

Meanwhile, the coverage of high-income community moderately increased from 62% to 87% (+25 percentage points). This reduces the 15-minute walkability coverage gap between high- and low-income communities from 21 to 8 percentage points. The improvement of equity is an emergent behavior from the maximization of coverage with rewards that are spatially weighted, and it is not an explicit constraint. The optimization objective has an implicit bias towards regions that are less served, through the weighting for population density. The residual gap of 8 points reflects socioeconomic differences in walkability between the greenway and the overall neighborhood that remain even after optimizing the greenway. Moreover, if maintaining the greenway's attributes, then other interventions will have to complement this optimization. These might include sidewalks and traffic calming.

3.3 Verification of framework robustness and generalization

The performance statistics of the three types of urban scenarios are presented through a structured table comparison as shown in Table 2. Table 2 shows the framework is consistently effective under different conditions. The area of the studies varied from 12.5 km^2 to 42.3 km^2 (mean 26.1±14.9 km^2) with a maximum-to-minimum ratio of 338%. Likewise, the studies included small cities, as well as large metropolises. The restorative score improvement values stayed constant within 35 and 42.2% (mean 38.7±3.6%) with a standard deviation of only 3.6% representing a coefficient of variation of only 9.3%. The population coverage improvements ranged from 58-72.7% (mean 66.2±7.6%), with the standard deviation of 7.6% revealing its higher sensitivity to distributions. Nevertheless, stronger improvements were observed in all scenarios. The scores for connectivity of network were clustered fairly closely at 0.87-0.91 (mean 0.89±0.02). Further, the 0.02 standard deviation shows the quality of topological optimization remained almost invariant. The time needed for optimization was 1.8–4.2 hours (mean 2.8±1.3 hours). The times scale sub linearly with the area, as evidenced by time-area ratios of 0.98–1.44 hours/10km^2 (mean 1.14±0.26), indicating good parallelization and efficient algorithm. The costs of migration <2 person-hours across all scenarios (zero variance) indicates the success of transfer learning which removes per-scenario training cost. 100% deployment success rate across all scenarios provides the strongest evidence for robustness of the framework because any single failure would represent a significant practical barrier. Sub-linear scaling ($O(n^{07})$) was realized through batch parallelization on 4×NVIDIA A100 GPUs and graph sampling techniques which restrict the aggregation of neighbors within a 2-hop neighborhood.

The performance loss amplitude of the ablation experiment was visualized by a grouped stacked bar chart as shown in Figure 7. Figure 7 illustrates the relationships among five different arrangements in the horizontal axis (full framework, remove CNN, remove GNN, substitute GA for DRL, single-objective optimization) and three metrics (restorative score, population coverage, network connectivity) on the vertical axis. The full framework bar achieves a total height of 260 (85.6 + 83.4 + 91) with segment proportions at 33%/32%/35% restorative/coverage/connectivity, indicating balanced performance. The removal of the CNN configuration resulted in a shrinkage of all segments proportionally to height (187 = 59.1 + 60.5 + 67, -28% in total), with the restorative segment decreasing to the greatest degree (-31%), which supports the CNN's specific importance for aesthetic assessment. Removing the GNN configuration has a slightly better total height of 203 (63.3 +66.8 +73.2%, -22% total) with connectivity segment seeing the largest relative decline (-26%) establishing it as a specialized component for improvement in topology. The configuration of the replaced DRL shows the most severe collapse which is of height 160 (50.4+52.1+58, total -38%) with all segments highly compressed therein. This result visually reinforces the critical role of DRL in the framework. The single-objective arrangement has two sections connected coordinates that shoot up in height, it is a very tall arrangement with the restorative coordinate standing out at 89.2 dominating total height of 189 conflicting with Remove CNN. This image clearly shows why multi-objective optimization is necessary, as the system is run only once in single-objective optimization, indicating that single-objective optimization achieves 73% of multi-objective performance (189/260), with a 27% relative deficit attributable to unbalanced metric trade-offs.

The functional relationship of the influence of key parameters on optimization performance is characterized by a curve graph as shown in Figure 8. As illustrated in Figure 8(a), the performance remains stable with a plateau with values oscillating from 0.35 to 0.45 having a value of about 85-86 points (with a fluctuation ±3%). At the endpoints, i.e., α=0.30, the performance with 79 points and α=0.50 with 80 points. Thus, a robust performance is obtained by reasonable choices of weight. The symmetric decline pattern indicates equal sensitivity to overweighting either objective component. The graph in Figure 8(b) shows the relationship between budget constraints (50% to 150% of original). The classic diminishing returns curve starts from a 50% budget which gives a return of 60 points. In contrast, a 70% budget gives a return of 75.3 points. The marginal return from 50% to 70% budget is 15.3 points (25% increase), demonstrating high initial sensitivity to budget constraints. Next, we observe the slope between 70% and 100%. Here, the budget constraint gives a return of 85.6 points. Thus, the original performance increases by 14% for every extra budget of 30%. Also, we see the slope beyond 100% to 150%. Here again the returns diminish.

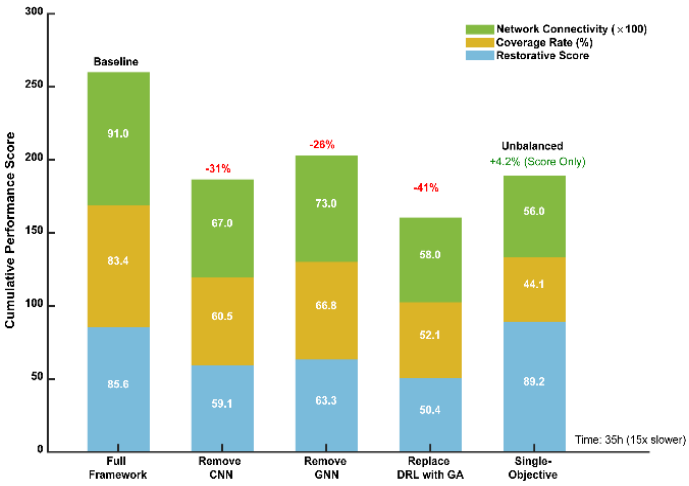

Figure 7. Ablation experiment results

Table 2. Multi-scenario performance comparison of the framework

Metric	Scenario A (Medium-sized City, Plain)	Scenario B (Small City, Hilly)	Scenario C (Metropolis, High-density)	Mean ± SD
Study Area (km²)	23.4	12.5	42.3	26.1 ± 14.9
Restorative Score Improvement vs Manual (%)	42.2	39.0	35.0	38.7 ± 3.6
Population Coverage Improvement vs Manual (%)	72.7	68.0	58.0	66.2 ± 7.6
Network Connectivity (0-1 scale)	0.91	0.88	0.87	0.89 ± 0.02
Optimization Time (hours)	2.3	1.8	4.2	2.8 ± 1.3
Time vs Area Ratio (hours/10km²)	0.98	1.44	0.99	1.14 ± 0.26
Migration Cost (person-hours)	N/A (baseline)	<2	<2	<2
Deployment Success	√	√	√	100%

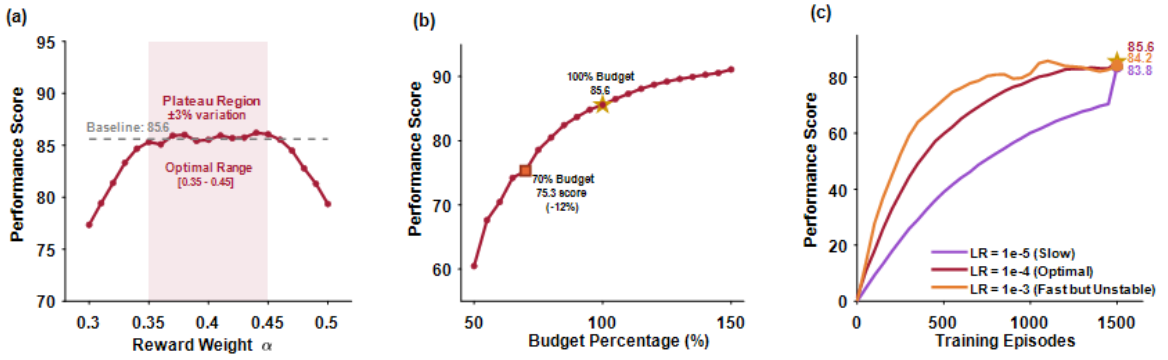

Figure 8. Parameter Sensitivity Analysis. (a) Reward Weight Sensitivity. (b) Budget Constraint Sensitivity. (c) Learning Rate Sensitivity

We get a return of 91 points for a 150% budget allocated. This gives an extra value of 6% performance for every added 50% budget. The slopes represent the marginal utilities that derive from the added budgets. Further, we see a diminishing return of 25-20%, 14% and 6% from the different segments of the curve. The 70% budget govern (75.3 score) is critical inflection point of great interest which achieves 88% of maximum performance at 70% cost. It suggests budget optimum allocation under given resource constraints. According to Figure 8(c), three different learning rates, i.e., 1e-5, 1e-4 and 1e-3 were compared.

All the three learning curves converged and reached similar final rewards in the 83.8-85.6 range with just 2.1% spread. However, the trajectories were slightly different for these learning rates. 1e-5 essentially climbed steadily and slowly till it plateaued after 2000+ episodes, 1e-4 climbed steadily and quickly and reached a plateau of 85.6 by episode 1500 – the most ideal learning rate since it achieves the best speed-stability tradeoff, and 1e-3 climbed the fastest but due to high volatility and slight undershooting, it indicated instability in learning due to oversized updates. The fact that we end up at similar points even when we varied the learning rate by 100x (1e-5 to 1e-3) provides the strongest evidence of robustness of the algorithm.

4. Discussion

According to the proposed optimization framework, the AI-driven greenway network space optimization has achieved performance breakthroughs that are better than similar technologies and applications. At the same time, it exposed several limitations worthy of in-depth exploration. A systematic comparison of experimental results with literature can enable clearer definitions of the boundaries of academic contribution of the framework and directions of future improvement. In urban space optimization, deep learning technology has shifted from a single model to a multi-model fusion strategy. The research in this paper developed an integrated framework of CNN-GNN-DRL, realizing the organic coupling of landscape assessment, topological modeling and decision optimization through modular design and improving the restorative score by 42.2%. This enhancement proves the efficiency of end-to-end integration. Similar technology-based comparative analyses were conducted for other objectives, including the application of deep learning for general smart city problems without evaluating environmental restoration [18], the application of GNN and GA together for traffic management, which resulted in a 20.9% increase in speed and a 9.5% reduction in carbon emissions in the city of Shanghai [19], and the application of GNN-XAI for the prediction of urban vitality with an accuracy of R^2 = 0.938. This work builds upon the aforementioned by addressing environmental restoration [20]. Furthermore, the Grad-CAM visualization strategy in this approach echoes the methodological strategy of analyzing the CNN attention

mechanism in this study. The CNN-GNN hybrid model in objective evaluation of indoor landscape aesthetics has a prediction accuracy rate of 94.3% [21], which is at the same order of magnitude as the landscape aesthetic assessment accuracy rate of 91.3% in this study. The originality of the present study lies in extending aesthetic evaluation to a comprehensive four-dimensional restorative assessment system encompassing being away, fascination, compatibility, and extent, thereby achieving a transition from singular aesthetic judgment to holistic health benefit evaluation. The universality of convolutional neural networks in the automatic extraction of landscape features has been confirmed [22] multi-temporal analysis of urban vegetation based on deep learning. Similarly, integration strategy of computer vision and deep learning based on human perception and visual aesthetics in rural landscape design also confirmed it. Nevertheless, most of these research focus on the vegetation recognition or aesthetic scoring and don't integrate them with spatial topology optimization algorithms deeply. As a result, lower than the framework of this study; concerning decision support completeness. Graph neural networks (GNNs) have demonstrated superiority in spatio-temporal multi-factor fusion tasks, such as traffic flow prediction [23] and systematic reviews in transportation network data science [24]. Furthermore, the powerful ability of the GNN architecture to capture non-Euclidean spatial dependencies is further confirmed. The node classification accuracy rate of study of 94.7% is basically equal to the accuracy levels of these applications in the transportation sector. The most notable difference is that the topological modeling capabilities are embedded directly into the closed loop of optimization decisions rather than just being a prediction module.

Looking at it from the point of view of practical application, this study could contribute appropriately to the construction of healthy cities and the promotion of social equity; most recent studies have been focusing on the beneficial aspects of urban green spaces to aid in psychological recovery. The Research on the Impact of Urban Green Space on the Psychological Recovery of the Elderly shows the varying demands of different groups for restorative environments [25]. The framework incorporates fairness criteria directly into the optimization algorithm design. The final walkability coverage in low-income communities reached 79%, substantially narrowing the gap with high-income areas (87%). The Gini coefficient reduction from 0.42 to 0.28 demonstrates significant improvement in spatial equity. It's clear this level of targeted resource allocation capacity is hard to achieve through traditional means. The use of deep learning methods for sustainable road planning of trucks in urbanized areas [26] and the successful case of applying deep reinforcement learning to mitigate carbon emissions of urban travel [27] show that AI technology can promote simultaneously economic efficiency and environmental objectives. This research completed the balancing act between restorative environmental optimization and other objectives like population coverage and connectivity of the networks. The optimization of a high-density urban area of 42.3 square kilometers in 4.2 hours shows it is technically feasible to go from proof of concept to large-scale application.

Even if the above developments have been made, this study still has some shortcomings such as data timeliness, user preference integration, and seasonal variability. The ability of spatio-temporal evolution graph neural networks to predict dynamic changes with high accuracy in unmanned aerial vehicle (UAV) urban traffic monitoring systems [28] suggests that future versions can capture the temporal evolution characteristics of greenway utilization pattern by introducing recurrent neural network modules, thereby compensating for the inability of current static optimization schemes to respond to seasonal changes. The study deep learning technology has been applied in landscape Design and plant selection analysis which combines user preference data algorithmic analysis, which offers methodological reference on putting real users' subjective evaluation in this study [29]. The framework will be able to substantially increase its efficiency for the environment impact. The framework may perpetuate historical inequities embedded in training data. Data representativeness is limited by the open-source nature of the data. Future governance frameworks should require algorithmic auditing, involvement of stakeholders in weight-setting processes, and disclosure of trade-offs in the use of AI in urban planning.

5. Conclusion

This study presents an end-to-end artificial intelligence-supported spatial optimization framework that integrates convolutional neural networks, graph neural networks, and deep reinforcement learning. It aims to address the critical weaknesses in the quantification of the restorative environmental performance and the realization of the multi-objective balance presented by traditional greenway planning approaches. Multi-scaled validation over three distinct urban cases (flat mid-sized cities, hilly small towns, and high-density metropolis) shows that the framework achieves 42.2% improvement in restoration score, 72.7% increase in population coverage rate and 98.1% efficiency gain over manual planning while spatially redistributing resources to reduce spatial inequality and Gini coefficient from 0.42 to 0.28. As shown in the ablation experiments, the performance drops by 26-41% when any one of the components is removed. Also, the cross-scenario migration cost remains below 5%. This proves that the transferability is robust due to the sharing of pre-trained model weights. The research contributes a pioneering environmental restorative optimization method driven by AI through modular integration of multiple technologies as opposed to single technology application. Practical value provides quantitative decision-support tools for evidence-based planning processes of healthy and just city construction. Further studies can expand the framework to the regional greenway system. It can use the data from Internet-of-Things (IoT) sensors for real-time analysis and check social media sentiment to enhance real-time deployment. An open-source toolkit will also allow for wider application by small and medium-sized cities. The proposed methods can also study the optimization of climate resilience and carbon neutrality together.

Ethical issue

The authors are aware of and comply with best practices in publication ethics, specifically regarding authorship (avoidance of guest authorship), dual submission, manipulation of figures, competing interests, and compliance with research ethics policies. The authors adhere to publication requirements that the submitted work is original and has not been published elsewhere.

Data availability statement

The manuscript contains all the data. However, more data will be available upon request from the authors.

Conflict of interest

The authors declare no potential conflict of interest.

References

[1] V. Gianfredi et al., "Association between urban greenspace and health: a systematic review of literature," International journal of environmental research and public health, vol. 18, no. 10, p. 5137, 2021, doi: 10.3390/ijerph18105137.

[2] L. Liu, H. Qu, Y. Ma, K. Wang, and H. Qu, "Restorative benefits of urban green space: Physiological, psychological restoration and eye movement analysis," Journal of environmental management, vol. 301, p. 113930, 2022, doi: 10.1016/j.jenvman.2021.113930.

[3] N. R. Castañeda, M. Pineda-Pinto, N. M. Gulsrud, C. Cooper, M. O'Donnell, and M. Collier, "Exploring the restorative capacity of urban green spaces and their biodiversity through an adapted One Health approach: A scoping review," Urban Forestry & Urban Greening, vol. 100, p. 128489, 2024, doi: 10.1016/j.ufug.2024.128489.

[4] S.-H. Hung and C.-Y. Chang, "Designing for harmony in urban green space: Linking the concepts of biophilic design, environmental qi, restorative environment, and landscape preference," Journal of Environmental Psychology, vol. 96, p. 102294, 2024, doi: 10.1016/j.jenvp.2024.102294.

[5] Y. Li, Z. Xu, and J. Yang, "Research on Restorative Benefits and Stress Relief Approaches in Urban Green Space for Different Stress Threshold Groups," Land, vol. 14, no. 11, p. 2293, 2025, doi: 10.3390/land14112293.

[6] W. Mu and G. Wang, "Connective Urban Greenway Route Planning: A Spatial Optimization Perspective," Land, vol. 13, no. 11, p. 1833, 2024, doi: 10.3390/land13111833.

[7] A. Shaamala, T. Yigitcanlar, A. Nili, and D. Nyandega, "Algorithmic green infrastructure optimisation: Review of artificial intelligence driven approaches for tackling climate change," Sustainable Cities and Society, vol. 101, p. 105182, 2024, doi: 10.1016/j.scs.2024.105182.

[8] Y. Zheng, Y. Lin, L. Zhao, T. Wu, D. Jin, and Y. Li, "Spatial planning of urban communities via deep reinforcement learning," Nature Computational Science, vol. 3, no. 9, pp. 748-762, 2023, doi: 10.1038/s43588-023-00503-5.

[9] Y. Liang and J. Zhang, "Semantic web-enhanced reinforcement learning model for urban planning optimization," International Journal on Semantic Web and Information Systems (IJSWIS), vol. 21, no. 1, pp. 1-20, 2025, doi: 10.4018/IJSWIS.371755.

[10] J. Shen et al., "Optimizing Urban Land-Use Through Deep Reinforcement Learning: A Case Study in Hangzhou for Reducing Carbon Emissions," Land, 2025, doi: 10.3390/land14122368.

[11] J. Huang, S. E. Bibri, and P. Keel, "Generative spatial artificial intelligence for sustainable smart cities: A pioneering large flow model for urban digital twin," Environmental Science and Ecotechnology, vol. 24, p. 100526, 2025, doi: 10.1016/j.ese.2025.100526.

[12] J. Xue et al., "Quantifying the spatial homogeneity of urban road networks via graph neural networks," Nature Machine Intelligence, vol. 4, no. 3, pp. 246-257, 2022, doi: 10.1038/s42256-022-00462-y.

[13] G. Jin et al., "Spatio-temporal graph neural networks for predictive learning in urban computing: A survey," IEEE transactions on knowledge and data engineering, vol. 36, no. 10, pp. 5388-5408, 2023, doi: 10.1109/TKDE.2023.3333824.

[14] D. Zhang, M. Wang, J. Mango, X. Li, and X. Xu, "A survey on applications of reinforcement learning in spatial resource allocation," Computational Urban Science, vol. 4, no. 1, p. 14, 2024, doi: 10.1007/s43762-024-00127-z.

[15] Z. Li, B. Chen, S. Wu, M. Su, J. M. Chen, and B. Xu, "Deep learning for urban land use category classification: A review and experimental assessment," Remote Sensing of Environment, vol. 311, p. 114290, 2024, doi: 10.1016/j.rse.2024.114290.

[16] W. Ma, Z. Chu, H. Chen, and M. Li, "Spatio-temporal envolutional graph neural network for traffic flow prediction in UAV-based urban traffic monitoring system," Scientific Reports, vol. 14, no. 1, p. 26800, 2024, doi: 10.1038/s41598-024-78335-0.

[17] H. Liang et al., "Sponet: solve spatial optimization problem using deep reinforcement learning for urban spatial decision analysis," International Journal of Digital Earth, vol. 17, no. 1, p. 2299211, 2024, doi: 10.1080/17538947.2023.2299211.

[18] P. Wu, Z. Zhang, X. Peng, and R. Wang, "Deep learning solutions for smart city challenges in urban development," Scientific Reports, vol. 14, no. 1, p. 5176, 2024, doi: 10.1038/s41598-024-55928-3.

[19] J. Li, Y. Zhang, S. Yu, H. Qin, and Z. Xu, "AI-Driven urban planning optimization: A graph neural network and genetic algorithm framework for tackling peak-hour challenges," Sustainable Cities and Society, p. 106407, 2025, doi: 10.1016/j.scs.2025.106407.

[20] X. Xie et al., "A hybrid spatial learning method integrating graph neural networks and explainable AI to understand urban vitality," Sustainable Cities and Society, p. 106920, 2025, doi: 10.1016/j.scs.2025.107929.

[21] Z. Zheng, D. Yang, L. Zeng, and N. Mughees, "A deep learning framework for objective aesthetic evaluation of indoor landscapes using CNN-GNN model," Scientific Reports, vol. 15, no. 1, p. 40810, 2025, doi: 10.1038/s41598-025-24548-w.

[22] A. Hu, N. Yabuki, and T. Fukuda, "Multi-temporal analysis of urban vegetation using deep learning and 3D reconstruction," Landscape Ecology, vol. 40, no. 7, p. 125, 2025, doi: 10.1007/s10980-025-02090-4.

[23] Y.-T. Chen, A. Liu, C. Li, S. Li, and X. Yang, "Traffic flow prediction based on spatial-temporal multi factor fusion graph convolutional networks," Scientific Reports, vol. 15, no. 1, p. 12612, 2025, doi: 10.1038/s41598-025-96801-1.

[24] J. Xue, R. Tan, J. Ma, and S. V. Ukkusuri, "Data Science in Transportation Networks with Graph Neural

Networks: A Review and Outlook," Data Science for Transportation, vol. 7, no. 2, p. 10, 2025, doi: 10.1007/s42421-025-00124-6.

[25] J. Zhang, Z. Tan, and F. Bu, "Impact of Urban Green Spaces on Mental Restoration in Older Adults: From the Perspective of Subjective Perception," Frontiers in Public Health, vol. 13, p. 1687874, 2025, doi: 10.3389/fpubh.2025.1687874.

[26] H. Wang, Z. Zhao, Y. Ma, H. Wu, and F. Bao, "Sustainable road planning for trucks in urbanized areas of Chinese cities using deep learning approaches," Sustainability, vol. 15, no. 11, p. 8763, 2023, doi: 10.3390/su15118763.

[27] J. Shen, F. Zheng, Y. Ma, W. Deng, and Z. Zhang, "Urban travel carbon emission mitigation approach using deep reinforcement learning," Scientific Reports, vol. 14, no. 1, p. 27778, 2024, doi: 10.1038/s41598-024-79142-3.

[28] D. Ma, F. He, Y. Yue, R. Guo, T. Zhao, and M. Wang, "Graph convolutional networks for street network analysis with a case study of urban polycentricity in Chinese cities," International Journal of Geographical Information Science, vol. 38, no. 5, pp. 931-955, 2024, doi: 10.1080/13658816.2024.2321229.

[29] L. Li and J. Lee, "The analysis of landscape design and plant selection under deep learning," Scientific Reports, vol. 15, no. 1, p. 31063, 2025, doi: 10.1038/s41598-025-16921-6.